frontiers | Frontiers in Physics

ORIGINAL RESEARCH
published: 25 July 2022
doi: 10.3389/fphy.2022.931419

Assessing Skin Healing and Angiogenesis of Deep Burns *in Vivo* Using Two-Photon Microscopy in Mice

*Gaiying He[1†], Yu Cao[2†], Jinghui Tang[3], Shuhua Ma[1], Yanan Sun[1], Weifeng Yang[1], Qian Tong[4], Dongying Li[1] and Yi Wang[1]**

[1]*Experimental Research Center, China Academy of Chinese Medical Sciences, Beijing, China,* [2]*Institute of Geriatrics, Xiyuan Hospital, China Academy of Chinese Medical Sciences, Beijing, China,* [3]*College of Chinese Medicine Materials, Jilin Agricultural University, Changchun, China,* [4]*School of Biological Engineering and Food Science, Hubei University of Technology, Hubei University of Technology, Wuhan, China*

Prevalent methods for monitoring burn injuries and testing drug efficacies rely on fixed tissue sections. However, this may leave out cellular details in the living state. *In vivo* assessments of burn healing has been long sought after and are of scientific and clinical interest. Nicotinamide adenine dinucleotide (phosphate) (NAD(P)H), collagen, and melanin are endogenous fluorescent molecules and their signals can be captured by two-photon microscopy (TPM), therefore providing information on epidermal histological features and collagen growth in real-time. In addition, TMP imaging on exogenous fluorescent substances provides a basis for detecting blood vessels. In this work, two-photon microscopy was used to capture the exogenous fluorescent substances and endogenous fluorescent molecules at different times to assess and track burn healing *in vivo*. Combining TPM imaging and morphological characteristics, proliferation and differentiation of the keratinocytes in different layers of skin, collagen contents, and angiogenesis were identified and quantified. The TPM monitoring method provides an effective tool to systemically evaluate skin healing of deep burns *in vivo*.

Keywords: deep burns, skin healing, angiogenesis, two-photon microscopy, *in vivo* imaging

OPEN ACCESS

Edited by:
Chao He,
University of Oxford, United Kingdom

Reviewed by:
Nan Zeng,
Tsinghua University, China
Yonghong He,
Tsinghua University, China

****Correspondence:***
Yi Wang
wangyi@merc.ac.cn

[†]These authors have contributed equally to this work

Specialty section:
This article was submitted to Optics and Photonics, a section of the journal Frontiers in Physics

Received: *29 April 2022*
Accepted: *13 June 2022*
Published: *25 July 2022*

Citation:
He G, Cao Y, Tang J, Ma S, Sun Y, Yang W, Tong Q, Li D and Wang Y (2022) Assessing Skin Healing and Angiogenesis of Deep Burns in Vivo Using Two-Photon Microscopy in Mice. Front. Phys. 10:931419. doi: 10.3389/fphy.2022.931419

1 INTRODUCTION

Burn injuries are one of the most common accidents that cause morbidity and mortality. Burn injuries, especially severe burns impose great burdens on both physical and mental health of the patient [1]. Burns are divided into three categories (first degree; superficial second degree and deep second degree; third-degree). Deep burns, including deep second-degree and third-degree wounds, damage the deep layer of the dermis. Burn healing process includes three stages, termed as: inflammatory (reactive), proliferative (reparative), and maturation (remodeling) phases with distinct biological characteristics. Drug misuse at improper stages may delay the healing process and cause microbial infections and scar formation. Therefore, identifying the different stages and pathological events in burn healing is the cornerstone of precise medicine.

Recently, non-invasive technologies have been developed to diagnose and classify burn injuries and monitor the burn healing *in vivo*, such as terahertz spectroscopy [2] and dual-scale photoacoustic imaging [3]. As far as we know, simultaneously assessing the epidermis,

extracellular matrix deposition, and angiogenesis in deep burns is deficient. Two-photon microscopy (TPM) is a high-resolution laser scanning imaging technique and a powerful tool to obtain *in vivo* quantifiable details of the skin. TPM has been extensively applied to study *in vivo* in inflammatory skin diseases [4, 5], skin aging [6–8], and transdermal drug deliveries [9, 10]. The penetration depth of TPM goes beyond the epidermis and superficial dermis to about 300–600 μm depending on the site, excitation wavelength, and fluorophores [11], compared with that of confocal microscopy, approximately 50–60 μm. TPM relies on the non-linear photoexcitation of molecules, whereby two low-energy photons are almost simultaneously absorbed in the same focal point, resulting in fluorescence emission [11]. Epidermal cells and extracellular matrices include a variety of endogenous fluorescent molecules, such as nicotinamide adenine dinucleotide (phosphate) (NAD(P)H), collagen, elastin, and melanin, which can be imaged by TPM non-invasively [12–14]. In addition, TMP imaging of exogenous fluorescent substances rhodamine–dextran provide important assessments for angiogenesis.

TPM imaging of NAD(P)H, collagen, and andrhodamine–dextran provided epidermal cells, dermal collagen, and blood vessels changes *in vivo*, which are important indicators of wound healing in deep burns. Therefore, we developed a method to provide real-time tracking of the burn healing process using TPM. *In vitro* pathological staining was employed as the gold standard to compare with the TPM results, regarding the evaluation of collagen contents and blood vessels. Our method may provide new insights in assessing skin healing and angiogenesis of deep burns *in vivo*.

2 MATERIALS AND METHODS

2.1 Animal Preparation

All animal experimental procedures were approved by the Institutional Animal Care and Use Committee of China Academy of Chinese Medical Sciences (protocol code ERCCACMS21-2016-10). 24 male C57BL/6 mice (20 ± 2 g), provided by Beijing Vital River Laboratory Animal Technology (Beijing, China), were randomly divided into two groups: burn group (Burn) and basic fibroblast growth factor (b-FGF) treatment group (Burn + b-FGF) with 12 in each group. Hair on the dorsal skin was shaved and depilated after anesthesia with isoflurane (Ruiward, Shenzhen, China). A burn model was established as reported by Tanaka and others with a slight modification [15]. Briefly, a 1-cm diameter circular wound was made on the back by water vapor heated to 96.5 °C at a water bath for 6 s. The wound was covered with Tegaderm™ transparent film (3M, Saint Paul, MN, USA). Three days later, excisions of the wounds were undertaken following a current clinical practice. b-FGF (150 IU/cm^2) was employed topically in the Burn + b-FGF group according to the instructions (Beijing Shuanglu Pharmaceutical, Beijing, China), and 0.9% physiologic saline was applied topically in the Burn group, once a day for 21 days.

2.2 Wound Healing Rate

Deep burn wounds were photographed on days 7, 14, and 21 with a rubber cushion of an inner diameter of 1.3 cm. The wound healing rate was calculated with ImageJ (National Institutes of Health), the following formula was used to calculate the wound healing rate.

$$\text{wound healing rate}\,(\%) = (A_0 - A_N)/A0.$$

A_0 was the wound area on day 0, A_N was the wound area on day N (7, 14, or 21).

2.3 TPM Imaging

In vivo imaging was done using a commercial two-photon excited fluorescence microscopy system (FV1000, Olympus, Japan) with a water-immersion objective lens (PLAN ×25 OB, Olympus, Japan) and a Ti: sapphire laser oscillator (MaiTai HP DS-OL, Spectra-Physics, CA). The excitation wavelength was tunable in visible and near-infrared spectrum (690–1,040 nm), which was suitable for detecting skin fluorescent molecules, such as adenine NAD(P)H, collagen, melanin, and elastin.

The mice were fixed to an object stage of TMP after anesthesia with isoflurane. The objective lens was immersed in water on the holder which sucked the skin to reduce the effect of breathing during measurements. Data were collected at the margin of the wound before re-epithelialization and at the center of wound after re-epithelialization on days 7, 14 and 21. The experimental scheme, procedure, and schematic illustration of the skin are shown in **Figure 1**. Pathological changes in the epidermis, dermis, and blood vessels were detected. NAD(P)H signal was detected at an excitation wavelength of 750 nm and emission wavelengths of 420–460 nm. Epidermal live cells were included in stratum granulosum, stratum spinosum, and stratum basale. Stratum basale is located at the deepest layer of the epidermis [16] and consists of columnar cells. Stratum granulosum lies in the outermost layer of the epidermis, the cells of stratum granulosum are larger than those of stratum spinosum. Previous studies distinguished stratum granulosum, stratum spinosum, and stratum basale and analyzed their pathological changes by TPM detection of NAD(P)H according to the localization and characteristics of living cells [4, 17]. The diameter and the number of epidermal skins were counted using ImageJ software. A collagen signal was detected at an excitation wavelength of 850 nm and emission wavelengths 420–460 nm. 3D reconstructions of the collagen were generated using Imaris software. The mean fluorescence intensity of the collagen fibers was calculated by dividing the total fluorescence intensity by fluorescence area. The density of the blood vessels was analyzed based on rhodamine–dextran (Sigma-Aldrich, Saint Louis, MO, USA) images. Briefly, rhodamine–dextran was injected in the tail vein of the mice, following a previously published protocol [6]. Images were collected at an excitation wavelength of 850 nm and emission filters of 495–540 nm. Rhodamine–dextran image sets were obtained comprised of TMP image stacks (90 μm) to assess angiogenesis. The image size was 1,024 × 1,024 pixels. Step size was 2.5 μm. The scanning speed of NAD(P)H and

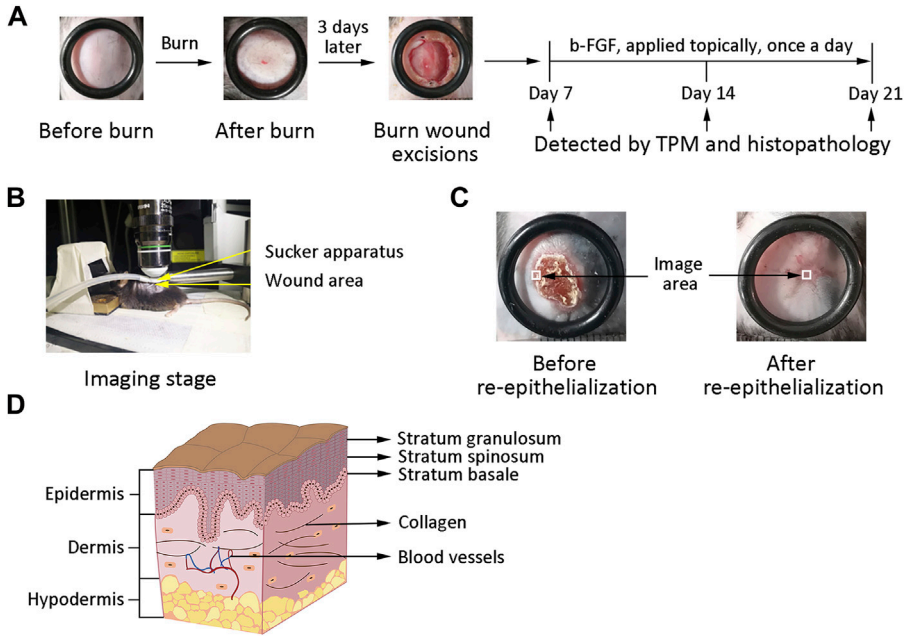

FIGURE 1 | Experimental scheme and schematic illustration of the skin. **(A)** Establishment of the deep-burn model and experimental scheme. **(B)** Anesthetized mouse on the imaging stage. Yellow arrows point at the sucker apparatus and wound area. **(C)** Imaging area at the margin before re-epithelialization and at the center of wound after re-epithelialization. The white square represents the imaging area. **(D)** Schematic illustration of the skin. Black arrows point at the different compositions of the skin.

collagen images was 4 μm/pixel, and that of rhodamine–dextran was 2 μm/pixel.

2.4 Staining

2.4.1 Hematoxylin and Eosin Staining

Burned skin was fixed in 4% paraformaldehyde (Solarbio, Beijing, China) for 48 h. Then, the specimens were paraffin-embedded and sectioned 6-μm in thickness with a microtome (Thermo Fisher Scientific, Waltham, MA, USA). Slices were stained with H and E and captured with a microscope (Olympus BX51, Tokyo, Japan).

2.4.2 Masson's Trichrome Staining

Tissues were fixed, paraffin-embedded, and sectioned. The collagen was stained with Masson staining reagent (Solarbio, Beijing, China), following a previously published protocol [18]. Finally, the images were captured with a microscope.

2.4.3 Toluidine Blue–Eosin Staining

Blood vessels were stained with toluidine blue and eosin after being fixed. Images of blood vessels were taken with a microscope.

2.5 Statistical Analyses

All data were expressed as mean ± standard deviation (SD). Data were analyzed by one-way ANOVA using SPSS v17.0 (IBM, Armonk, NY, United States). Graphs were created using Prism v6.0 (GraphPad, La Jolla, CA, USA). $p < 0.05$ was considered significant.

3 RESULTS

3.1 Wound Healing of Deep Burns in Mice

To evaluated wound changes on days 7, 14, and 21, the wound in each group was photographed (**Figure 2A**) and the wound healing rate was analyzed (**Figure 2B**). On day 7, the wound area of the Burn + b-FGF group was reduced significantly than that of the Burn group ($p < 0.01$). On day 14, the wound in the Burn group did not heal, whereas the wounds in the Burn + b-FGF group had healed completely ($p < 0.01$). On day 21, the wound in each group had healed, but the scar area treated by b-FGF was less than that in the Burn group. These results suggested that b-FGF could accelerate the healing of deep burns in mice.

3.2 Epidermal Healing of Deep Burns in Mice

To evaluate the epidermal healing of deep burns *in vivo*, we tracked the cell morphology of stratum granulosum, and the cell numbers of stratum spinosum and stratum basale throughout the 21 days. Different layers were recognized according to the characteristics and location of the cells obtained by NAD(P)H imaging. The reconstructions of the different layers of epidermis are shown in **Figure 3A**.

To examine cell morphology of stratum granulosum, we imaged the cell of stratum granulosum by NAD(P)H imaging in normal skin (**Figure 3B**), the Burn group, and the Burn + b-FGF group at different days (**Figure 3C**). The cell mean diameter of stratum granulosum was calculated (**Figure 3D**).

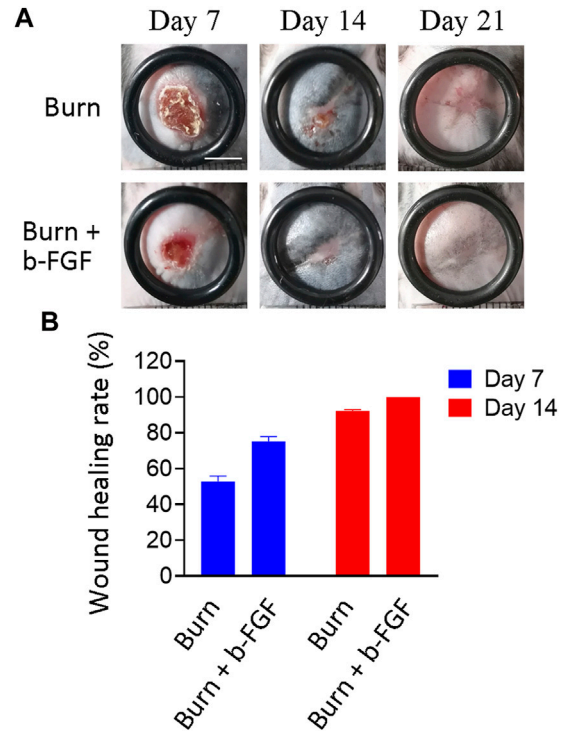

FIGURE 2 | Wound healing of deep burns in mice. **(A)** Images of the deep burns in different groups. Scale bar = 50 mm. **(B)** Wound healing rate of the deep burns was measured (n = 6).

The epidermis had virtually no cells of stratum granulosum at the wound margin in the Burn group and Burn + b-FGF group on day 7 (the images are not shown). On day 14, the cell diameter of stratum granulosum was larger in the Burn + b-FGF group than that of the Burn group, however, without statistical significance. On day 21, the cell diameters of stratum granulosum were 15.34 ± 0.56 and 22.24 ± 1.11 μm in the Burn group and Burn + b-FGF group, respectively, with statistical significance ($p < 0.05$).

To further explore keratinocyte proliferation and differentiation of stratum spinosum and stratum basale in deep burns, cell numbers were counted by obtaining *in vivo* NAPDH signals. **Figures 3E,F** show the representative NAD(P)H images of stratum spinosum in normal skin and deep burns selected from one field of view from 170 μm × 170 μm images (**Supplementary Figure S1A**). The cell number of stratum spinosum from NAD(P)H images were calculated (**Figure 3G**). Representative NAD(P)H images of stratum basale in normal skin (**Figure 3H**) and deep burn (**Figure 3I**) were shown selected one field from 170 μm × 170 μm images (**Supplementary Figure S1B**). The cell number was calculated (**Figure 3J**). Cells of stratum spinosum and stratum basale from NADPH images were sparse on day 7. On day 14, the number of cells in the stratum spinosum and stratum basale were increased significantly compared with the Burn group ($p < 0.05$). On day 21, the intercellular space was reduced significantly, the cell number of stratum spinosum and stratum basale increased by 1.37-fold ($p < 0.05$) and 1.43-fold ($p < 0.01$) after b-FGF treatment. These results showed that the proliferation and differentiation of an epidermal cell can be detected and quantified *in vivo* by NAD(P)H imaging using TMP.

3.3 Collagen Production in the Dermis of Deep Burns in Mice

In order to explore collagen production, we observed the features of collagen growth and quantitatively analyzed the mean fluorescence intensity. 3D reconstructions of the collagen were obtained in normal skin (**Figure 4A**), the Burn group, and the Burn + b-FGF group at different days (**Figure 4B**). Mean fluorescence intensity presented in **Figure 4B** was calculated (**Figure 4C**).

The collagen fibers showed centripetal growth, parallel and loose arrangement, and less mean fluorescence intensity of the collagen fibers at the margin of the wound site in both groups before re-epithelialization. On day 14, re-epithelialization in the Burn group had not completed, and the collagen continued to grow centripetally. The re-epithelialization in the Burn + b-FGF group had completed, however, the mean fluorescence intensity did not show statistical differences between the Burn group and the Burn + b-FGF group. On day 21, the mean fluorescence intensity of the Burn + b-FGF group increased significantly compared with that of the Burn group, with statistical significance ($p < 0.05$). We further evaluated the collagen change by Masson staining. Representative Masson staining images were obtained in normal skin (**Figure 4D**), the Burn group, and the Burn + b-FGF group at different days (**Figure 4E**). Results showed collagen volume fraction (CVF) was low in the Burn group and the Burn + b-FGF group on days 7 and 14. On day 21, the CVF of the Burn + b-FGF group increased significantly compared with that of the Burn group (**Figure 4F**, $p < 0.01$). Masson staining results were consistent with TMP imaging. The aforementioned results showed that the changes of collagen could be detected and quantified *in vivo* using TMP.

3.4 Angiogenesis of Deep Burns in Mice

TMP imaging detects exogenous fluorescent substances as well as endogenous fluorescent molecules, which provides the basis for detecting blood vessels *in vivo*. In order to assess angiogenesis of deep burns in mice, we injected rhodamine–dextran into the tail vein and obtained the rhodamine–dextran image sets. We quantitatively analyzed the density of rhodamine–dextran image sets during wound healing. Representative rhodamine–dextran images sets were obtained in normal skin (**Figure 5A**), the Burn group, and the Burn + b-FGF group at different days (**Figure 5B**). The density of the blood vessels from rhodamine–dextran images presented in **Figure 5B** were calculated (**Figure 5C**).

Rhodamine–dextran from TMP imaging showed that blood vessels grew toward the wound before re-epithelialization. The density of the blood vessels in the Burn + b-FGF group increased

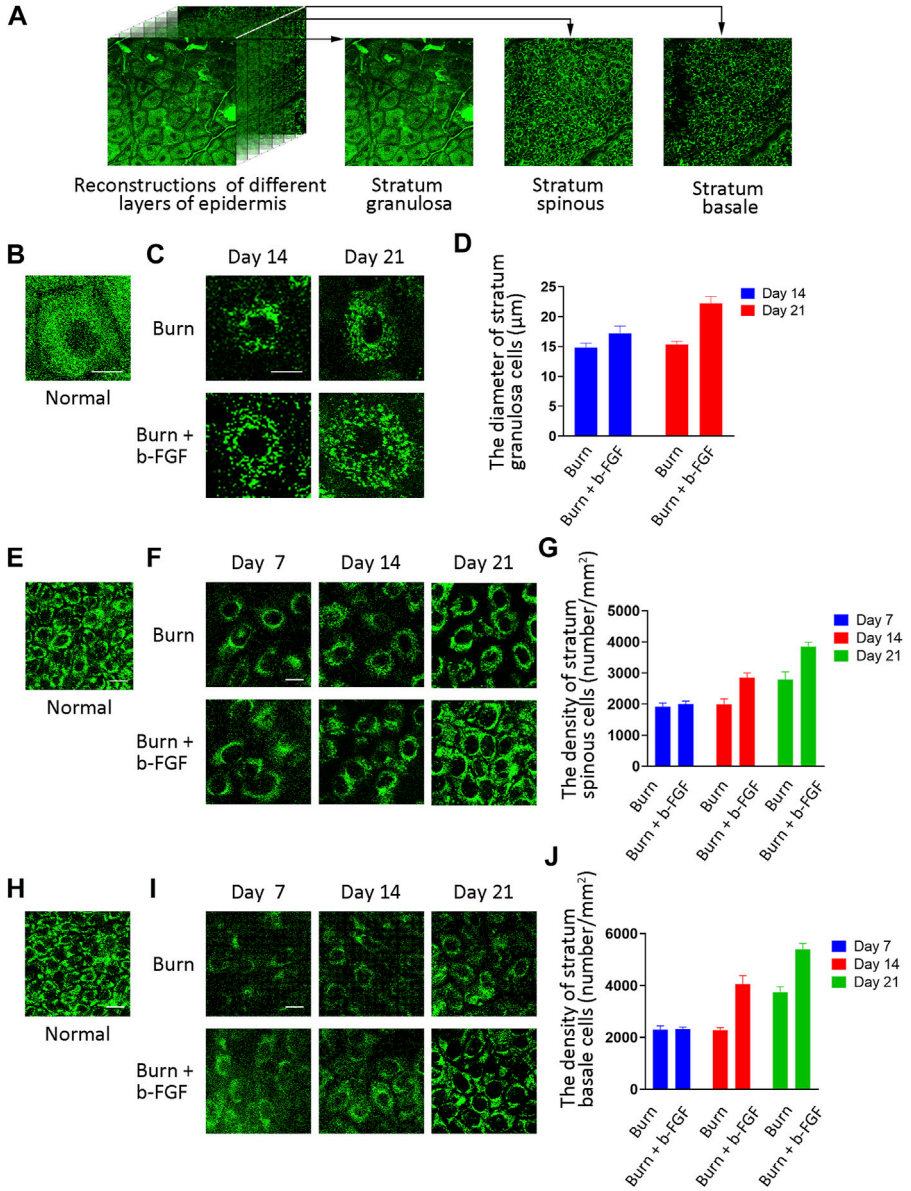

FIGURE 3 | Epidermal healing assessment of the deep burns from NAD(P)H images by TPM in mice. **(A)** Reconstructions of different layers of the epidermis. **(B)** Cell morphology of the stratum granulosum from NAD(P)H images in normal skin. The area of NAD(P)H images was 33 μm × 33 μm. Scale bar = 10 μm. **(C)** Cell morphology of the stratum granulosum from NAD(P)H images between the Burn group and the Burn + b-FGF group. The area of NAD(P)H images was 33 μm × 33 μm. Scale bar = 10 μm. **(D)** Cell diameter of stratum granulosum was calculated. **(E)** Images of stratum spinosum from NAD(P)H images in normal skin. The area of the NAD(P)H images was 56 μm × 56 μm. Scale bar = 10 μm. **(F)** Images of stratum spinosum from the NAD(P)H images between the Burn group and the Burn + b-FGF group. The area of the NAD(P)H images was 56 μm × 56 μm. Scale bar = 10 μm. **(G)** Image number of stratum spinosum was calculated. **(H)** Cells of stratum basale from NAD(P)H images in normal skin. The area of NAD(P)H images was 56 μm × 56 μm. Scale bar = 10 μm. **(I)** Cells of stratum basale from the NAD(P)H images between the Burn group and the Burn + b-FGF group. The area of the NAD(P)H images was 56 μm × 56 μm. Scale bar = 10 μm. **(J)** Cell number of stratum basale was calculated.

markedly than the Burn group on day 7 ($p < 0.05$). On day 14, the density of the blood vessels in the Burn + b-FGF group significantly increased than that of the Burn group, with statistical significance ($p < 0.05$). On day 21, the density of the blood vessels in the Burn + b-FGF group was 1.69-fold than that of the Burn group ($p < 0.05$). To further explore the changes in the blood vessels by pathological staining, we examined toluidine blue–eosin staining in normal skin (**Figure 5D**), the Burn group, and the Burn + b-FGF group at different days (**Figure Figure5E**). The number of blood vessels in the Burn + b-FGF group significantly increased than the Burn group on days 14 and 21 (**Figure 5F**, $p < 0.05$). The results of toluidine blue–eosin staining were consistent with the TPM imaging. These results showed the imaging of rhodamineVdextran by TMP provided an important method for assessing the angiogenesis of deep burns.

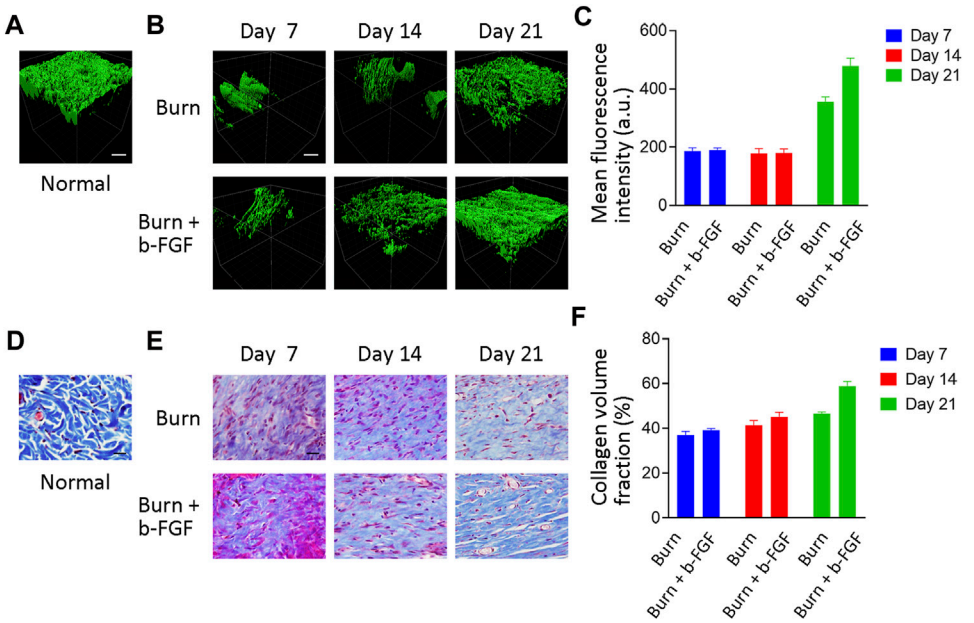

FIGURE 4 | Collagen production assessment of the deep burns by TPM and Masson staining in mice. **(A)** 3D reconstructions of collagen were generated using Imaris software in normal skin. Scale bar = 30 μm. **(B)** 3D reconstructions of collagen were generated using Imaris software between the Burn group and the Burn + b-FGF group. Scale bar = 30 μm. **(C)** Mean fluorescence intensity of collagen was analyzed from TMP imaging. **(D)** Collagen images of tissue slices detected by Masson staining in normal skin. Scale bar = 20 μm. **(E)** Collagen images of tissue slices detected by Masson staining between the Burn group and the Burn + b-FGF group. Scale bar = 20 μm. **(F)** CVF was analyzed from Masson staining.

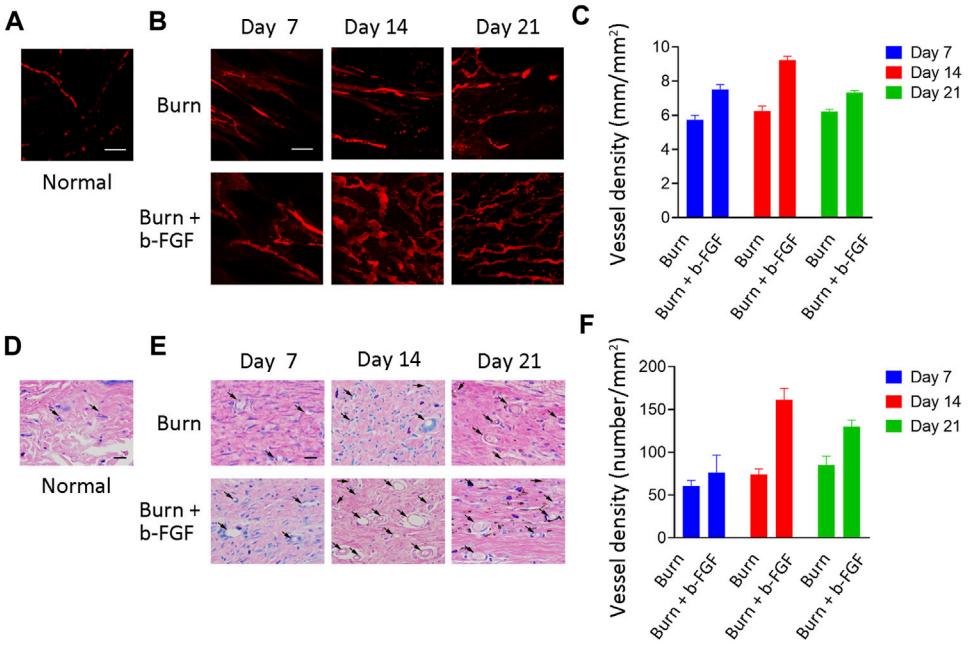

FIGURE 5 | Angiogenesis assessment of the deep burns by TPM and toluidine blue–eosin staining in mice. **(A)** Blood vessel image sets obtained *in vivo* which comprised of the TMP image stack in normal skin. Scale bar = 50 μm. **(B)** Blood vessel image sets obtained *in vivo* which were comprised of the TMP image stack between the Burn group and the Burn + b-FGF group. Scale bar = 50 μm. **(C)** Mean density of the blood vessels was analyzed from rhodamine–dextran imaging. **(D)** Blood vessel images of skin slices detected by toluidine blue–eosin staining in normal skin. Scale bar = 20 μm. **(E)** Blood vessels images of skin slices detected by Toluidine blue–eosin staining between the Burn group and the Burn + b-FGF group. Scale bar = 20 μm. **(F)** Number of blood vessels was analyzed from toluidine blue–eosin staining.

4 DISCUSSION

In this work, TPM was used for *in vivo* tracking the healing process in deep burns by capturing the florescent signals of epidermal NAD(P)H and dyes in the vessel. Recently, TPM imaging has been used in skin diseases *in vivo* due to deep penetration into tissue, low energy, and high sensitivity [11, 19, 20], which overcome the shortcomings of traditional sectioning, staining, and antibody labeling.

Burn healing process is a multi-step process consisting of the inflammatory, proliferation, and remodeling phases. The inflammatory phase is defined as a temporal activation and recruitment of various cells of innate and adaptive immunity. The proliferative phase is vital for wound closure, involving keratinocytes, endothelial cells, fibroblasts proliferation, and granulation tissue formation. The remodeling phase lasts weeks to months and is characterized by wound contraction and scar maturation [21]. In the study, we mainly focused on the proliferation phase that is vital to burn healing. Epidermal cell proliferation and differentiation, collagen contents, and changes of the blood vessels establishing blood circulation were detected with TPM *in vivo* to manifest this phase. Furthermore, b-FGF was used as a positive control which is widely used for deep burns. Previous studies have found that b-FGF reduced the total duration of therapy by accelerating the time of re-epithelialization or healing time [22], increasing collagen contents [23, 24], and regulating angiogenesis [25]. Therefore, its effects were observed and specified in different aspects during the proliferation phase of burn healing.

Re-epithelialization is considered as a key step in wound healing because it generates a new barrier between the denuded surface and the environment. The epidermis is composed of stratum granulosum, stratum spinosum, and stratum basale from stratum corneum consisting of dead cells [26]. Only basal keratinocytes can proliferate and give rise to differentiated descendants [27]. The normal architecture of the stratum granulosum appears to be lost next to the wound site, but the granular layer is increasingly normalized away from the wound [28]. The cells of stratum granulosum in normal skin/mature skin have a larger body and continuous arrangement [4, 28]. The cell of stratum granulosum is large and its morphological changes represent epidermal differentiation and the mature state. So far, the repair process of the stratum granulosum, stratum spinosum, and stratum basale cannot be evaluated well using traditional methods *in vivo*; however it can be detected using TPM. Different layers of the skin can be classified according to the characteristics and location of the epidermal cell. In this work, we explore the cell number of different layers of the epidermis according to NAD(P)H images *in vivo*. The results found that b-FGF accelerated cell proliferation and differentiation of stratum spinosum and stratum basale, and increased the cell size of stratum granulosum indicating a well-differentiated epidermis, which demonstrated that b-FGF accelerates re-epithelialization.

The collagen, accounting for 70–80% of dry skin weight, is the main component of the extracellular matrix [29, 30] and can be employed as an indicator in the process of dermal repair. Collagen imaging has been widely used in the transdermal movement of drugs *in vivo* [31], scar prognosis [32, 33], and cancerous tissues [34, 35]. This study showed that b-FGF accelerated collagen production by TMP imaging *in vivo*, which was consistent with the Masson staining results *in vitro*. In addition, TMP imaging of collagen found that newly grown collagen fibers showed centripetal growth, parallel, and loose arrangement before re-epithelialization. The aforementioned results showed that the changes of collagen can be detected and quantified *in vivo* by collagen imaging using TMP.

Angiogenesis is an important sign of wound healing [36, 37], which maintains the growth of new granulation tissue and ensures the survival of keratinocytes around wounds by increasing the oxygen and nutrient supply [38]. Traditional *ex vivo* methods of vessel identification rely on immunochemistry and histological features [39, 40]; however, they omit real-time details. This study found that rhodamine–dextran from TMP images quantitatively assessed angiogenesis of deep burns established blood perfusion *in vivo* in deep burns, and revealed the dynamic changes of blood vessels during healing.

TPM is used for *in vivo* tracking the effects of b-FGF in deep burns by epidermal cell proliferation and differentiation, collagen contents, and angiogenesis. However, the effects of b-FGF on epidermis, collagen, and blood vessels are different at different times. The results showed that b-FGF promoted epidermal cell proliferation and differentiation on days 7, 14, and 21. Due to the limited imaging area of TPM, we only captured the partial collagen fibers at the margin of the wound. We found that collagen fibers showed the centripetal growth at the margin of the wound, and there was no difference in collagen content during the healing process on day 7 and 14. However, on day 21 after the healing, we found that b-FGF promoted the regeneration of collagen at the center of the wound by TPM imaging. TPM imaging showed that b-FGF promoted angiogenesis on days 7, 14, and 21. When re-epithelialization was completed, the density of blood vessels decreased. Therefore, on day 21, vascular density was decreased significantly in the Burn group and the Burn + b-FGF group than that of on day 14. In conclusion, b-FGF accelerates epidermis proliferation and differentiation, collagen contents, and angiogenesis at different times.

The TPM monitoring method provides an effective tool to systemically evaluate skin healing of deep burns *in vivo*. However, two-photon imaging has disadvantages that limit its application [1]. Two-photon-only images endogenous fluorescent molecules and second harmonic substances, and other substances were not evaluated [2]. The imaging area of TPM is limited, which omitted partial useful information. We believe that TPM provides more information on evaluating skin healing with the development of TPM imaging technology.

5 CONCLUSION

We performed a longitudinal study to track skin and blood vessel changes of deep burns during wound healing. By TMP imaging exogenous fluorescent substances and endogenous fluorescent molecules, we have directly detected epidermal cells, dermal collagen, and micro-vessel changes. TMP imaging assesses

epidermal healing by cell proliferation and differentiation. To investigate the changes of extracellular matrix, we imaged collagen, an important indicator of dermal repair. TMP imaging showed collagen contents and grew centripetally. The TMP imaging detects exogenous fluorescent substances, such as rhodamine–dextran to provide changes in the blood vessels of established blood circulation. These results highlight that TMP imaging can be a powerful *in vivo* method to assess the skin healing process in deep burns.

DATA AVAILABILITY STATEMENT

The original contributions presented in the study are included in the article/**Supplementary Material**; further inquiries can be directed to the corresponding author.

ETHICS STATEMENT

The animal study was reviewed and approved by the Institutional Animal Care and Use Committee of China Academy of Chinese Medical Sciences (protocol code ERCCACMS21-2016-10).

AUTHOR CONTRIBUTIONS

GH and YW designed the study, reviewed, and revised the manuscript. GH and YC drafted the initial manuscript. JT and SM performed the measurements for the study. YS and WY coordinated and supervised data collection. QT and DL critically reviewed the manuscript for important intellectual content. All authors approved the final manuscript as submitted and agree to be accountable for all aspects of the work.

FUNDING

The Fundamental Research Funds for the Central Public Welfare Research Institutes (ZZ2018018, XTCX2021002, JBGS2021007, ZZ13-YQ-077).

SUPPLEMENTARY MATERIAL

The Supplementary Material for this article can be found online at: https://www.frontiersin.org/articles/10.3389/fphy.2022.931419/full#supplementary-material

REFERENCES

1. Jeschke MG, van Baar ME, Choudhry MA, Chung KK, Gibran NS, Logsetty S. Burn Injury. *Nat Rev Dis Primers* (2020) 6(1):11. doi:10.1038/s41572-020-0145-5
2. Osman OB, Jack Tan T, Henry S, Warsen A, Farr N, McClintic AM, et al. Differentiation of Burn Wounds in an *In Vivo* Porcine Model Using Terahertz Spectroscopy. *Biomed Opt Express* (2020) 11(11):6528–35. doi:10.1364/BOE.397792
3. Wu Z, Duan F, Zhang J, Li S, Ma H, Nie L. *In Vivo* dual-scale Photoacoustic Surveillance and Assessment of Burn Healing. *Biomed Opt Express* (2019) 10(7):3425–33. doi:10.1364/BOE.10.003425
4. Huck V, Gorzelanny C, Thomas K, Getova V, Niemeyer V, Zens K, et al. From Morphology to Biochemical State - Intravital Multiphoton Fluorescence Lifetime Imaging of Inflamed Human Skin. *Sci Rep* (2016) 6:22789. doi:10.1038/srep22789
5. Kim B, Lee SH, Yoon CJ, Gho YS, Ahn G-O, Kim KH. *In Vivo* visualization of Skin Inflammation by Optical Coherence Tomography and Two-Photon Microscopy. *Biomed Opt Express* (2015) 6(7):2512–21. doi:10.1364/BOE.6.002512
6. Miyamoto K, Kudoh H. Quantification and Visualization of Cellular NAD(P)H in Young and Aged Female Facial Skin within Vivotwo-Photon Tomography. *Br J Dermatol* (2013) 169(Suppl. 2):25–31. doi:10.1111/bjd.12370
7. Miler I, Rabasovic MD, Aleksic M, Krmpot AJ, Kalezic A, Jankovic A, et al. Polarization-resolved SHG Imaging as a Fast Screening Method for Collagen Alterations during Aging: Comparison with Light and Electron Microscopy. *J Biophotonics* (2021) 14(3):e202000362. doi:10.1002/jbio.202000362
8. Czekalla C, Schönborn K-H, Döge N, Jung S, Darvin ME, Lademann J, et al. Impact of Body Site, Age, and Gender on the Collagen/Elastin Index by Noninvasive *In Vivo* Vertical Two-Photon Microscopy. *Skin Pharmacol Physiol* (2017) 30(5):260–7. doi:10.1159/000477854
9. Pappinen S, Pryazhnikov E, Khiroug L, Ericson MB, Yliperttula M, Urtti A. Organotypic Cell Cultures and Two-Photon Imaging: Tools for *In Vitro* and *In Vivo* Assessment of Percutaneous Drug Delivery and Skin Toxicity. *J Controlled Release* (2012) 161(2):656–67. doi:10.1016/j.jconrel.2012.03.005
10. Santos MA, Goertz DE, Hynynen K. Focused Ultrasound Hyperthermia Mediated Drug Delivery Using Thermosensitive Liposomes and Visualized with *In Vivo* Two-Photon Microscopy. *Theranostics* (2017) 7(10):2718–31. doi:10.7150/thno.19662
11. Obeidy P, Tong PL, Weninger W. Research Techniques Made Simple: Two-Photon Intravital Imaging of the Skin. *J Invest Dermatol* (2018) 138(4):720–5. doi:10.1016/j.jid.2018.01.017
12. Sarri B, Chen X, Canonge R, Grégoire S, Formanek F, Galey J-B, et al. *In Vivo* quantitative Molecular Absorption of Glycerol in Human Skin Using Coherent Anti-stokes Raman Scattering (CARS) and Two-Photon Auto-Fluorescence. *J Controlled Release* (2019) 308:190–6. doi:10.1016/j.jconrel.2019.07.018
13. Czekalla C, Schönborn KH, Lademann J, Meinke MC. Noninvasive Determination of Epidermal and Stratum Corneum Thickness *In Vivo* Using Two-Photon Microscopy and Optical Coherence Tomography: Impact of Body Area, Age, and Gender. *Skin Pharmacol Physiol* (2019) 32(3):142–50. doi:10.1159/000497475
14. Alex A, Chaney EJ, Žurauskas M, Criley JM, Spillman DR, Hutchison PB, et al. *In Vivo* characterization of Minipig Skin as a Model for Dermatological Research Using Multiphoton Microscopy. *Exp Dermatol* (2020) 29(10):953–60. doi:10.1111/exd.14152
15. Li C, Sun Y, Yang W, Ma S, Zhang L, Zhao J, et al. Pilose Antler Extracts (PAEs) Protect against Neurodegeneration in 6-OHDA-Induced Parkinson's Disease Rat Models. *Evidence-Based Complement Altern Med* (2019) 2019:1–11. doi:10.1155/2019/7276407
16. Blaydon DC, Kelsell DP. Defective Channels lead to an Impaired Skin Barrier. *J Cel Sci* (2014) 127(Pt 20):4343–50. doi:10.1242/jcs.154633
17. Žurauskas M, Barkalifa R, Alex A, Marjanovic M, Spillman DR, Jr., Mukherjee P, et al. Assessing the Severity of Psoriasis through Multivariate Analysis of Optical Images from Non-lesional Skin. *Sci Rep* (2020) 10(1):9154. doi:10.1038/s41598-020-65689-4
18. Yergoz F, Hastar N, Cimenci CE, Ozkan AD, Tekinay T, Guler MO, et al. Heparin Mimetic Peptide Nanofiber Gel Promotes Regeneration of Full Thickness Burn Injury. *Biomaterials* (2017) 134:117–27. doi:10.1016/j.biomaterials.2017.04.040
19. Jeong S, Hermsmeier M, Osseiran S, Yamamoto A, Nagavarapu U, Chan KF, et al. Visualization of Drug Distribution of a Topical Minocycline Gel in Human Facial Skin. *Biomed Opt Express* (2018) 9(7):3434–48. doi:10.1364/BOE.9.003434

20. Haluszka D, Lőrincz K, Kiss N, Szipőcs R, Kuroli E, Wikonkál N, et al. Diet-induced Obesity Skin Changes Monitored by *In Vivo* SHG and *Ex Vivo* CARS Microscopy. *Biomed Opt Express* (2016) 7(11):4480–9. doi:10.1364/Boe.7.004480
21. El Ayadi A, Jay JW, Prasai A. Current Approaches Targeting the Wound Healing Phases to Attenuate Fibrosis and Scarring. *Int J Mol Sci* (2020) 21(3):1105. doi:10.3390/ijms21031105
22. Ahn H-n., Kang H-s., Park S-j., Park M-h., Chun W, Cho E. Safety and Efficacy of Basic Fibroblast Growth Factors for Deep Second-Degree Burn Patients. *Burns* (2020) 46(8):1857–66. doi:10.1016/j.burns.2020.06.019
23. Otani Y, Komura M, Komura H, Ishimaru T, Konishi K, Komuro H, et al. Optimal Amount of Basic Fibroblast Growth Factor in Gelatin Sponges Incorporating β-Tricalcium Phosphate with Chondrocytes. *Tissue Eng A* (2015) 21(3-4):627–36. doi:10.1089/ten.TEA.2013.0655
24. Chakrabarti S, Mazumder B, Rajkonwar J, Pathak MP, Patowary P, Chattopadhyay P. bFGF and Collagen Matrix Hydrogel Attenuates Burn Wound Inflammation through Activation of ERK and TRK Pathway. *Sci Rep* (2021) 11(1):3357. doi:10.1038/s41598-021-82888-9
25. Tran-Nguyen T-M, Le K-T, Nguyen L-GT, Tran T-LT, Hoang-Thai P-C, Tran TL, et al. Third-degree Burn Mouse Treatment Using Recombinant Human Fibroblast Growth Factor 2. *Growth Factors* (2020) 38(5-6):282–90. doi:10.1080/08977194.2021.1967342
26. Ter Horst B, Chouhan G, Moiemen NS, Grover LM. Advances in Keratinocyte Delivery in Burn Wound Care. *Adv Drug Deliv Rev* (2018) 123:18–32. doi:10.1016/j.addr.2017.06.012
27. Hu Y, Baud V, Oga T, Kim KI, Yoshida K, Karin M. IKKα Controls Formation of the Epidermis Independently of NF-Kb. *Nature* (2001) 410(6829):710–4. doi:10.1038/35070605
28. Chang S-C, Chiang C-P, Lai C-H, Du P-WA, Hung Y-S, Chen Y-H, et al. Matriptase and Prostasin Proteolytic Activities Are Differentially Regulated in normal and Wounded Skin. *Hum Cel* (2020) 33(4):990–1005. doi:10.1007/s13577-020-00385-z
29. Varani J, Spearman D, Perone P, Fligiel SEG, Datta SC, Wang ZQ, et al. Inhibition of Type I Procollagen Synthesis by Damaged Collagen in Photoaged Skin and by Collagenase-Degraded Collagen *In Vitro*. *Am J Pathol* (2001) 158(3):931–42. doi:10.1016/S0002-9440(10)64040-0
30. Park SJ, Lee M, Yun JM, Kim D, Lee J, Lee YH. Zingiber Mioga Extract Improves Moisturization and Depigmentation of Skin and Reduces Wrinkle Formation in UVB-Irradiated HRM-2 Hairless Mice. *Appl Sciences-Basel* (2021) 11(3):976. doi:10.3390/app11030976
31. Kuo T-R, Wu C-L, Hsu C-T, Lo W, Chiang S-J, Lin S-J, et al. Chemical Enhancer Induced Changes in the Mechanisms of Transdermal Delivery of Zinc Oxide Nanoparticles. *Biomaterials* (2009) 30(16):3002–8. doi:10.1016/j.biomaterials.2009.02.003
32. Chen G, Chen J, Zhuo S, Xiong S, Zeng H, Jiang X, et al. Nonlinear Spectral Imaging of Human Hypertrophic Scar Based on Two-Photon Excited Fluorescence and Second-Harmonic Generation. *Br J Dermatol* (2009) 161(1):48–55. doi:10.1111/j.1365-2133.2009.09094.x
33. Pham TT, Hong EM, Moy WJ, Zhao J, Hu AC, Barnes CH, et al. The Biophysical Effects of Localized Electrochemical Therapy on Porcine Skin. *J Dermatol Sci* (2020) 97(3):179–86. doi:10.1016/j.jdermsci.2020.01.006
34. Scodellaro R, Bouzin M, Mingozzi F, D'Alfonso L, Granucci F, Collini M, et al. Whole-Section Tumor Micro-architecture Analysis by a Two-Dimensional Phasor-Based Approach Applied to Polarization-dependent Second Harmonic Imaging. *Front Oncol* (2019) 9:527. doi:10.3389/fonc.2019.00527
35. Sibai M, Mehidine H, Moawad EK, Juchaux M, Varlet P, Devaux B, et al. Comparison of Optically-Derived Biomarkers in Healthy and Brain Tumor Tissue under One- and Two-Photon Excitation. *J Biophotonics* (2019) 12(11):e201900111. doi:10.1002/jbio.201900111
36. Nagaraja S, Chen L, DiPietro LA, Reifman J, Mitrophanov AY. Predictive Approach Identifies Molecular Targets and Interventions to Restore Angiogenesis in Wounds with Delayed Healing. *Front Physiol* (2019) 10:636. doi:10.3389/fphys.2019.00636
37. Rahman MS, Islam R, Rana MM, Spitzhorn LS, Rahman MS, Adjaye J, et al. Characterization of Burn Wound Healing Gel Prepared from Human Amniotic Membrane and Aloe Vera Extract. *BMC Complement Altern Med* (2019) 19:115. doi:10.1186/s12906-019-2525-5
38. Johnson KE, Wilgus TA. Vascular Endothelial Growth Factor and Angiogenesis in the Regulation of Cutaneous Wound Repair. *Adv Wound Care* (2014) 3(10):647–61. doi:10.1089/wound.2013.0517
39. Michalczyk ER, Chen L, Maia MB, DiPietro LA. A Role for Low-Density Lipoprotein Receptor-Related Protein 6 in Blood Vessel Regression in Wound Healing. *Adv Wound Care* (2020) 9(1):1–8. doi:10.1089/wound.2019.1019
40. Duchesne C, Banzet S, Lataillade JJ, Rousseau A, Frescaline N. Cold Atmospheric Plasma Modulates Endothelial Nitric Oxide Synthase Signalling and Enhances Burn Wound Neovascularisation. *J Pathol* (2019) 249(3):368–80. doi:10.1002/path.5323

Conflict of Interest: The authors declare that the research was conducted in the absence of any commercial or financial relationships that could be construed as a potential conflict of interest.